Failure analysis on laminate structures of windsurfing boards using thin film modelling techniques

N. Schwarzer, Saxonian Institute of Surface Mechanics, 04838 Eilenburg, Am Lauchberg 2, Germany, Fax: ++493423656666, Tel: ++493423656639
E-Mail: n.schwarzer@esae.de

P. Heuer-Schwarzer, ESAE, Am Lehmberg 11, 04838 Eilenburg, Germany, Fax: ++493423604159, Tel: ++491773844847, E-Mail: p.heuer@esae.de

Abstract

Within this paper recently developed mathematical tools for the modelling of contact problems on thin film structures [1] for multilayers and gradient coatings are adapted to allow the investigation of laminate structures of transversal isotropy.
Applying series approaches using Bessel and Sinus functions complete three dimensional solutions can be found for relatively complex laminate structures allowing to model quasistatic contact, impact and bending loads. Worked into a small computer program the approach can be used to model laminate structures with up to 100 different layers on an ordinary personal computer in an acceptable calculation time.
The new tool is applied to analyse a variety of load problems typically occurring in windsurfing and leading to damage of the boards consisting of a laminated shell and an polymer foam core.

Keywords: Fibres, Foams, Layered Structures, Anisotropy, Fracture, Mechanical Properties, Analytical Modelling

Introduction

Laminate structures are playing an important role everywhere it comes to combine lightness and flexibility with high stability and reliability. So numerous publications are available treating laminate composites with respect to the latter quality characteristics. The reader may

find a very comprehensive introduction into the effect of impact and bending loads on laminate structure in [2].

A short survey concerning the accuracy and the calculation time shall present the development of the approach used here. Applying the model of the layered half space and using the method of image loads or image contacts, Schwarzer has been able to model up to 4 layers including the substrate [3]. The approach brought very good agreement with experimental results in the case of single layer and bi-layer structures, but unfortunately it is not applicable on real multilayers with more than 5 layers. The main reason for this is due to the high calculation time increasing exponentially with the number of layers. The same respectively similar facts hold for some other methods like the perturbation [4] or the boundary and the finite element method [5]. There is a variety of publications about multilayered and graded coatings available [6 - 9], but none of them provides a sufficiently convenient and fast method allowing to treat contact problems on mixed pure and transversely isotropic or transversely isotropic laminate structures under contact loading as we want to consider here. Especially if one wants to optimise laminate structures against impact and bending loads sufficiently fast evaluating approaches are required allowing to model contact problems on multi-layer structures for isotropy and transverse isotropy with a high number of relatively thin layers. It has been shown by Stone [10] (see also [11] and [12]), that in the case of a layered half space a sufficiently high number of layers can be modelled due to the method of integral transformation. He even modelled mixed pure and transversely isotropic layer structures under normal stress distribution. However in those cases, where the laminate structure is thin or in about the same scale as the area of the load applied on the laminated body in question, this method is not applicable due to numerical instabilities. So, if one for example wants to model impact and bending loads on unsupported thin film structures, multilayer coatings on thin substrates, hulls of boats, fuselages or other rather thin walled constructions the so called “model of the thick plate” is required. Thus, based on the approach of Lurie [13] Schwarzer [14] has developed a model allowing the investigation of thick layered plates under any arbitrary contact or bending load. The model has been included into a computer program evaluating mixed pure isotropic and transversely isotropic laminate

structures with up to 100 different layers on an ordinary personal computer in an acceptable calculation time.

Theory – The Model of the Thick Layered Plate

Apart from finite element or boundary element methods the integral transform method seems to be the only one allowing real multilayer modelling with more than 10 layers. As we are here only interested in contact areas of symmetry of revolution, we seek for a solution of the Navier equation for equilibrium in linear elasticity (see e.g. [10]) containing Bessel functions. However, in order to obtain numerically stable approaches in the case of laminate structures being thin compared to the size of the contact zone (or in about the same scale), the integral transformation method [15] must be substituted by a suitable series procedure. Thus, the method is based upon the following approach for circular contact areas where, in the case of pure isotropy, the displacements within the i-th layer is given by:

$$\vec{u}_i = \begin{pmatrix} u_i \\ v_i \\ w_i \end{pmatrix} = \sum_{n=1}^{\infty} c_n \begin{pmatrix} u^2\left(\left(A+B+Buz\right)e^{uz} - \left(D-F+Fuz\right)e^{-uz}\right)J_1[ur]\dfrac{x}{r} \\ u^2\left(\left(A+B+Buz\right)e^{uz} - \left(D-F+Fuz\right)e^{-uz}\right)J_1[ur]\dfrac{y}{r} \\ u^2\left(\left(-A+\left(2-4\nu-uz\right)B\right)e^{uz} - \left(D+\left(2-4\nu+uz\right)F\right)e^{-uz}\right)J_0[ur] \end{pmatrix} \tag{1}$$

$J_n(z)$ denotes the Bessel function of the first kind of order n, x, y, z are the Cartesian co-ordinates with z being the axis of indentation and $r^2=x^2+y^2$.

For transverse isotropic layers the approach must read:

$$\vec{u}_i = \begin{pmatrix} u_i \\ v_i \\ w_i \end{pmatrix} = \sum_{n=1}^{\infty} c_n \begin{pmatrix} u^2\left(Ae^{uz/\gamma_1} + Be^{uz/\gamma_2} - \left(De^{-uz/\gamma_1} + Fe^{-uz/\gamma_2}\right)\right)J_1[ur]\dfrac{x}{r} \\ u^2\left(Ae^{uz/\gamma_1} + Be^{uz/\gamma_2} - \left(De^{-uz/\gamma_1} + Fe^{-uz/\gamma_2}\right)\right)J_1[ur]\dfrac{y}{r} \\ u^2\left(m_1\left(\dfrac{A}{\gamma_1}e^{uz/\gamma_1} + \dfrac{D}{\gamma_1}e^{-uz/\gamma_1}\right) + m_2\left(\dfrac{B}{\gamma_2}e^{uz/\gamma_2} + \dfrac{F}{\gamma_2}e^{-uz/\gamma_2}\right)\right)J_0[ur] \end{pmatrix} \tag{2}$$

The parameter u must be set $u = \frac{\lambda_n}{r_0}$, with λ_n denoting the n-th root of the equation $J_0(r)=0$.

The parameter r_0 must be chosen such, that it is big compared to the lateral dimensions of the investigated laminate part and sufficiently small in order to reduce the number of terms of the series approach necessary to generate a proper surface load distribution. In the calculations presented here, up to 1000 terms were used. The γ_k (k=1, 2) have to be obtained from $\gamma_k^2=n_k$, whereas n_k denote the two (real or conjugate complex) roots of the equation

$$A_{11}A_{44}n^2 + \left[A_{13}\left(A_{13}+2A_{44}\right) - A_{11}A_{33}\right]n + A_{33}A_{44} = 0\,. \tag{3}$$

The constants m_k (k=1, 2) are related to γ_k as

$$\frac{A_{11}\gamma_k^{\,2} - A_{44}}{A_{13}+A_{44}} = \frac{\left(A_{13}+A_{44}\right)\gamma_k^{\,2}}{A_{33} - \gamma_k^{\,2}A_{44}} = m_k \tag{4}$$

Rearranging all terms of (2) containing γ_1 and denoting the resulting function F_1 and doing the same with all term containing γ_2 obtaining a function F_2 the elastic field can be evaluated due to:

$$u + iv \equiv u^c = \Lambda\left(F_1 + F_2 + iF_3\right);\ \Lambda = \frac{\partial}{\partial x} + i\frac{\partial}{\partial y}\quad ;\ w = m_1\frac{\partial F_1}{\partial z} + m_2\frac{\partial F_2}{\partial z}\,. \tag{5}$$

$$\sigma_1 = 2A_{66}\frac{\partial^2}{\partial z^2}\left(\left[\gamma_1^{\,2} - \left(1+m_1\right)\gamma_3^{\,2}\right]F_1 + \left[\gamma_2^{\,2} - \left(1+m_2\right)\gamma_3^{\,2}\right]F_2\right), \tag{6}$$

$$\sigma_2 = 2A_{66}\Lambda^2\left(F_1+F_2\right), \tag{7}$$

$$\sigma_{zz} = A_{44}\frac{\partial^2}{\partial z^2}\left(\gamma_1^{\,2}\left(1+m_1\right)F_1 + \gamma_2^{\,2}\left(1+m_2\right)F_2\right), \tag{8}$$

$$\tau_z = A_{44}\Lambda\frac{\partial}{\partial z}\left(\left(1+m_1\right)F_1 + \left(1+m_2\right)F_2\right), \tag{9}$$

($\gamma_3^2=A_{44}/A_{66}$). To simplify the stress field the following combinations were used (Fabrikant [16])
$\sigma_1=\sigma_{xx}+\sigma_{yy}=\sigma_{rr}+\sigma_{\varphi\varphi}$, $\sigma_2=\sigma_{xx}-\sigma_{yy}+2i\tau_{xy}=e^{2i\varphi}\left(\sigma_{rr}-\sigma_{\varphi\varphi}+2i\tau_{r\varphi}\right)$, $\tau_z=\tau_{xz}+i\tau_{yz}=e^{i\varphi}\left(\tau_{rz}+i\tau_{\varphi z}\right)$.

The yet unknown constants A,B, D and F have to be determined for each layer due to the boundary conditions at the interfaces of the multilayer structure. From equations (2) and (5) the complete elastic field at any point within the loaded laminate structure can be evaluated

applying the formulae (6) to (9). For more information the reader is referred to the original works of Schwarzer [1, 2, 3], Stone [10] and Fabrikant [16].

In the case of square contact regions the approach above must be changed as follows:
For isotropy:

$$\vec{u}_i = \sum_{n,m=1}^{\infty} c_{n,m} \begin{pmatrix} au\left(\left(A+B+Buz\right)e^{uz} - \left(D-F+Fuz\right)e^{-uz}\right)\sin\left[ax\right]\cos\left[by\right] \\ bu\left(\left(A+B+Buz\right)e^{uz} - \left(D-F+Fuz\right)e^{-uz}\right)\cos\left[ax\right]\sin\left[by\right] \\ u^2\left(\left(-A+\left(2-4\nu-uz\right)B\right)e^{uz} - \left(D+\left(2-4\nu+uz\right)F\right)e^{-uz}\right)\cos\left[ax\right]\cos\left[by\right] \end{pmatrix}, \quad (10)$$

where a and b have to be read as a_n and b_m with setting them $a_n=\pi*n/r_0$ and $b_m=\pi*m/r_0$. In addition we have $u^2=a^2+b^2$.
For transverse isotropic layers the approach must read:

$$\vec{u}_i = \sum_{n,m=1}^{\infty} c_{n,m} \begin{pmatrix} au\left(Ae^{uz/\gamma_1} + Be^{uz/\gamma_2} - \left(De^{-uz/\gamma_1} + Fe^{-uz/\gamma_2}\right)\right)\sin\left[ax\right]\cos\left[by\right] \\ bu\left(Ae^{uz/\gamma_1} + Be^{uz/\gamma_2} - \left(De^{-uz/\gamma_1} + Fe^{-uz/\gamma_2}\right)\right)\cos\left[ax\right]\sin\left[by\right] \\ u^2\left(m_1\left(\frac{A}{\gamma_1}e^{uz/\gamma_1} + \frac{D}{\gamma_1}e^{-uz/\gamma_1}\right) + m_2\left(\frac{B}{\gamma_2}e^{uz/\gamma_2} + \frac{F}{\gamma_2}e^{-uz/\gamma_2}\right)\right)\cos\left[ax\right]\cos\left[by\right] \end{pmatrix} \quad (11)$$

The evaluations are straight forward but tedious. Thus, two special software packages have been developed in order to automate the calculations becoming immensely complex and cumbersome in the case of high numbers of layers [17, 18].

Application to a variety of board failure problems in windsurfing

Windsurfing – some basics and the equipment

The first prototype of a sailboard dates back to the late 1950's, when the founding father of windsurfing, Newman Darby, wanted to combine sailing and wave surfing in one movement. The first windsurf board was about 3.5m long and weighted 27kg. Since then, many things changed: as the material and shapes of the equipment changed constantly, heavy and unwieldy polyethylene boards belong to the past, the jumps and moves become more and

more radical and windsurfing is nowadays one of the most popular watersports all over the world.

Windsurf equipment consists of two major parts: the complete rig with a mast making the rig stand upright, a sail to catch the wind, turn it into sail force and drive the craft, and a boom which spreads the sail and on which the windsurfer holds on, gives direction and controls the wind pressure/speed.

The second part of the vehicle is the board:

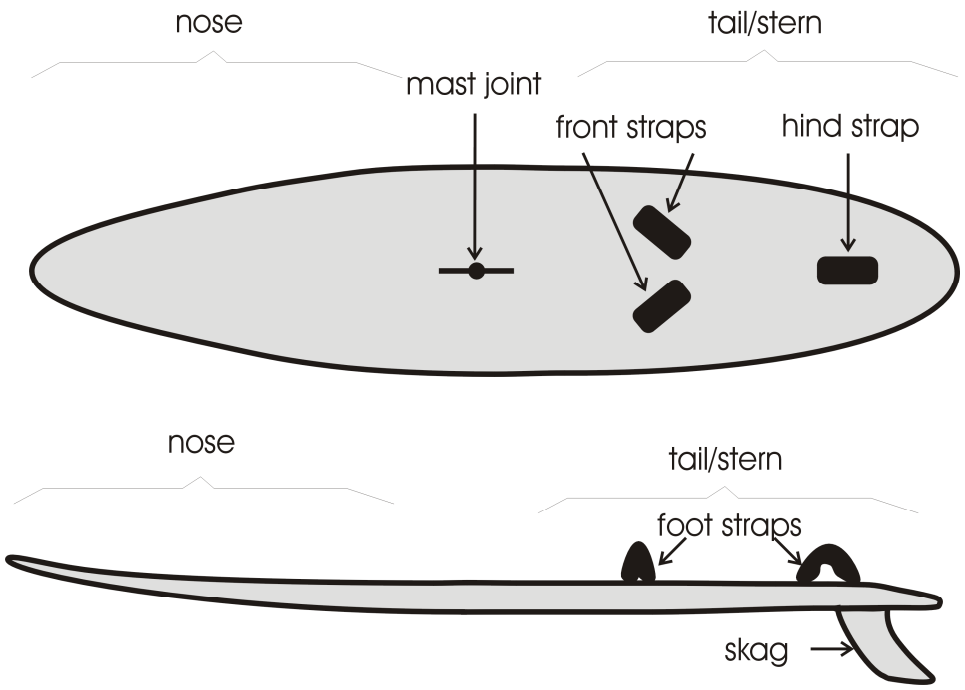

Fig. 1 Main parts of a windsurfing board

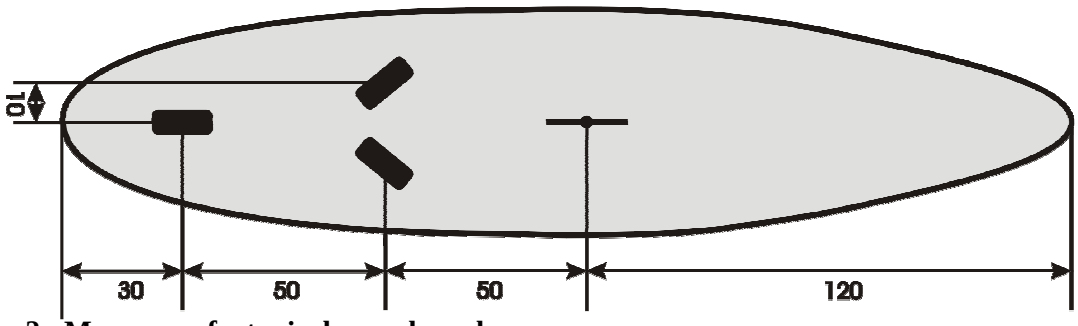

Fig. 2 Measures of a typical wave board

The bow is very often called the board's nose and is bent slightly upwards. On the stern, also called tail, are three foot straps located, two front, and one hind strap, in which the rider (windsurfer) finds a foothold when sailing fast and jumping. A certain area under those foot straps is covered with rubber foot pads, making it more comfortable for the surfer, preventing him from slipping and finally protecting the board against hard impact. A tail fin, or skag, is the main lateral pressure centre under water and thus, sets up resistance against drifting off course. Depending on the purpose and shape, a modern typical wave board weights about 8 kg and has a length of 2.6m to 2.8m.

Both parts, rig and board, are connected by a flexible mast joint that allows the rig to be tilted in any direction. By tilting the rig and with that, changing the incidence angle toward the wind, the sail force is moved whereas the lateral pressure centre (skag and all parts under water) stays the same and thus the board can be steered easily and without a rudder.

With a harness, which connects the rider's waist to the sail, the advanced windsurfer can transfer the power from the wind pressure caught in his sail to his body and with that, the required muscle power in hands and arms reduce to a bearable minimum so that even light female windsurfers, even if very rare, can practice this interesting sport without problems.

When the windsurfer gets faster, he is able to climb his own bow wave that his board produced when moving and thus, edging out water, and he will ride down this bow wave and becomes even faster. This state is called "planning" and now the rider can crawl into the foot straps and do different speed moves and jumps.

Fig. 3 Number one reason for board failure: jumps

Some of the most popular and spectacular movements are so called loop jumps. Therefore, the rider jumps high into the air and turns his rig, his board and himself either forward or backward so that he lands -if all goes well- after a full rotation in riding direction. But those moves are not only spectacular and create a stir, but they are also dangerous for both: the windsurfer and the equipment.

Board failure problems

A thorough analysis of the failure problems observable on windsurfing boards as given in [2] shows that there are two major mechanisms leading to damage. First, there are impact loads. They are mainly induced due to so called flat landing after high jumps. Here, the rider lands his board flat on the water surface and thus produces a momentarily high impulse under his feet and the board mast joint. There also catapult like plunges due to strong gusts pulling the rig and sometimes also the rider (who is fixed to the rig with the harness) strongly forward. This can lead to forceful hits with front parts of the boom or body parts of the rider onto the surface of the nose part of the board. The second class of main failure mechanism are bending loads coming from overturning of so called loop jumps, landing between waves or so called nose or tail dives after high jumps.
Due to the limitation of space we here concentrate on the impact loading conditions leading to damage directly caused by the mechanical contact. Within this class of failure mechanisms we here concentrate on the following critical situations:

1. impact load on the board's nose surface due to hard contact with either body parts of the rider or the rig
2. impact load in the foot pads area (under the foot straps) due to flat landing
3. skag hits reef

During our investigation we had to realise that in almost all cases of board destruction it was rather impossible to reconstruct the force and momentum situation in the moment of failure in detail. This was mainly due to the fact that the riders could only give vague information about their speed, height of the jump, buffer effect of the sail during lading, momentum of rotation etc. or in same cases even their own weight. Further, the investigated boards, though in principle of similar shape and structure differed widely in details concerning the number of uses laminate reinforcements, thicknesses of distinct parts of the boards, used materials within

the layered structure and their order (glass fibre, carbon fibre, honeycomb reinforcements…) etc.. Under these circumstances it doesn't seem reasonable to assume concrete load conditions and board constructions. One rather should apply typical load distributions simulating the critical situations and see whether or not the resulting stress distributions coincide with the observed board failure. Thus, we have contracted a relatively simple "model windsurfing board" out of either a layered half space or a layered thick plate model in accordance with the load problem in question. In order to describe board reinforcements in lateral direction a stability weight function had been introduced in case 3. This weight function is directly related to the lateral change of thickness of the laminate structure.

The first two problems 1 and 2 can be tackled by applying a half space or a thick plate model. We use the material parameters given in table 1 and 2. As explained above we are just interested in the resulting stress distribution and not any absolute values. Thus, the coefficients of the Young's modulus tensor are given as a function of a parameter E, where a concrete number can be assigned to as soon as concrete board structures are chosen and absolute forces are known. For the resulting stress distribution however, only the geometrical conditions and the relative material properties of the layers are of importance.

At first we investigate the effect of the impact load on the foam core of the board.

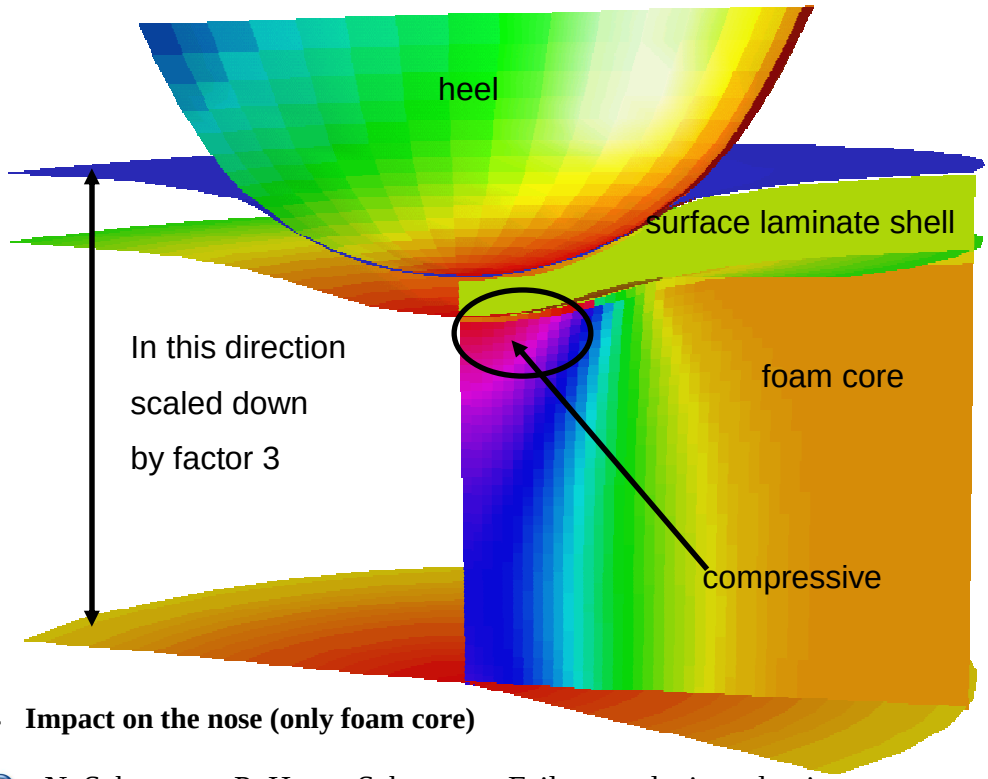

Fig. 4 Impact on the nose (only foam core)

As we know from investigating damaged boards, the foam is compressed under the contact zone. It often delaminates from the laminate surface (monochrome layer in fig. 4) thus, building a vacancy and leaving the laminate shell unsupported. The figure shows the hydrostatic stress having a strong maximum directly under the indenter (e.g. heel of the rider or front part of the boom…) leading to the material compression. In figure 5 the radial stress within the laminate shell is presented.

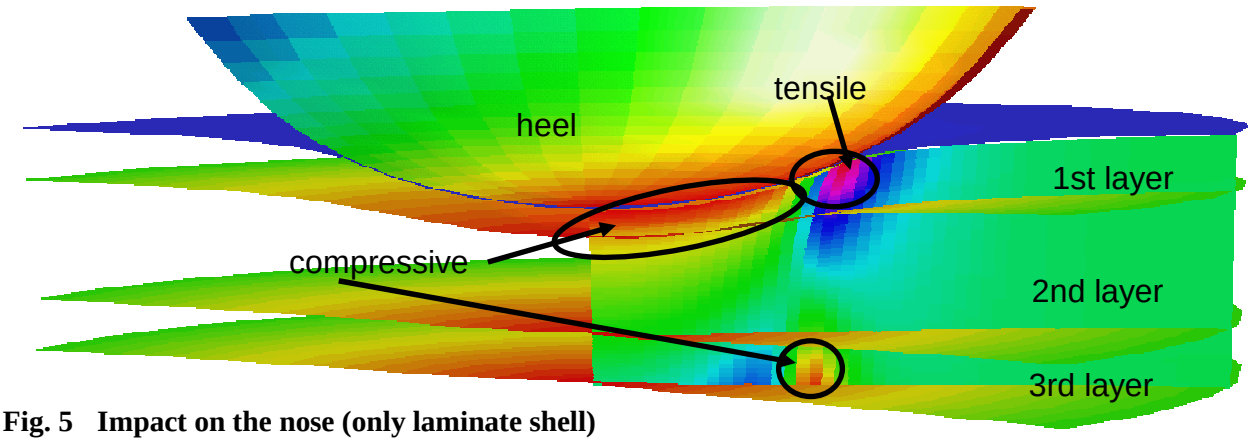

Fig. 5 Impact on the nose (only laminate shell)

It shows a pronounced tensile stress maximum at the contact rim which might lead to mode I fracture (Hertzian cone crack). And in fact this type of failure could be observed rather often on the front surface part of windsurfing boards:

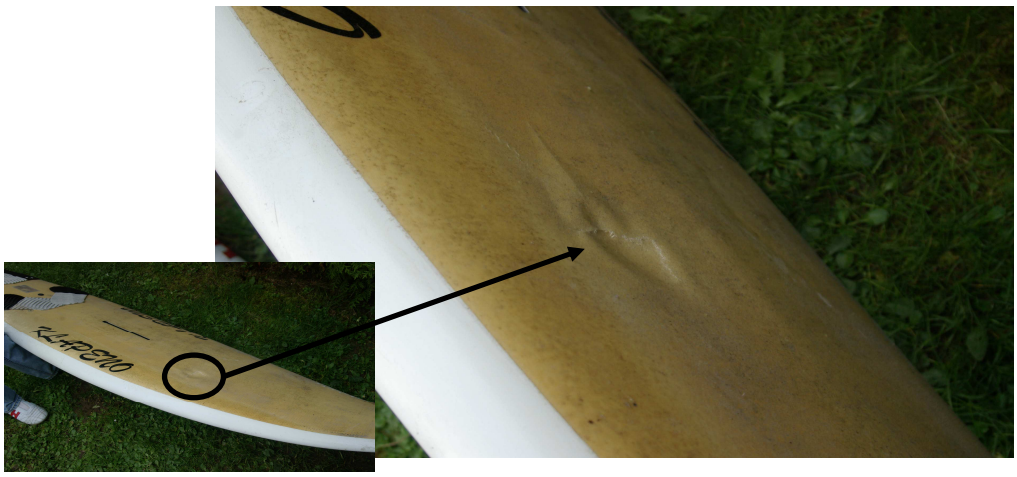

Fig. 6 Surface fracture damage due to impact load

This failure behaviour is well known from layered structures of hard thin films deposited on relatively soft substrates. Here too one often finds Hertzian-like fracture of the coating (e.g. [19]).

Back to the windsurfing boards: The picture changes completely when the impact load is applied onto the foot pad area (problem 2: figure 7):

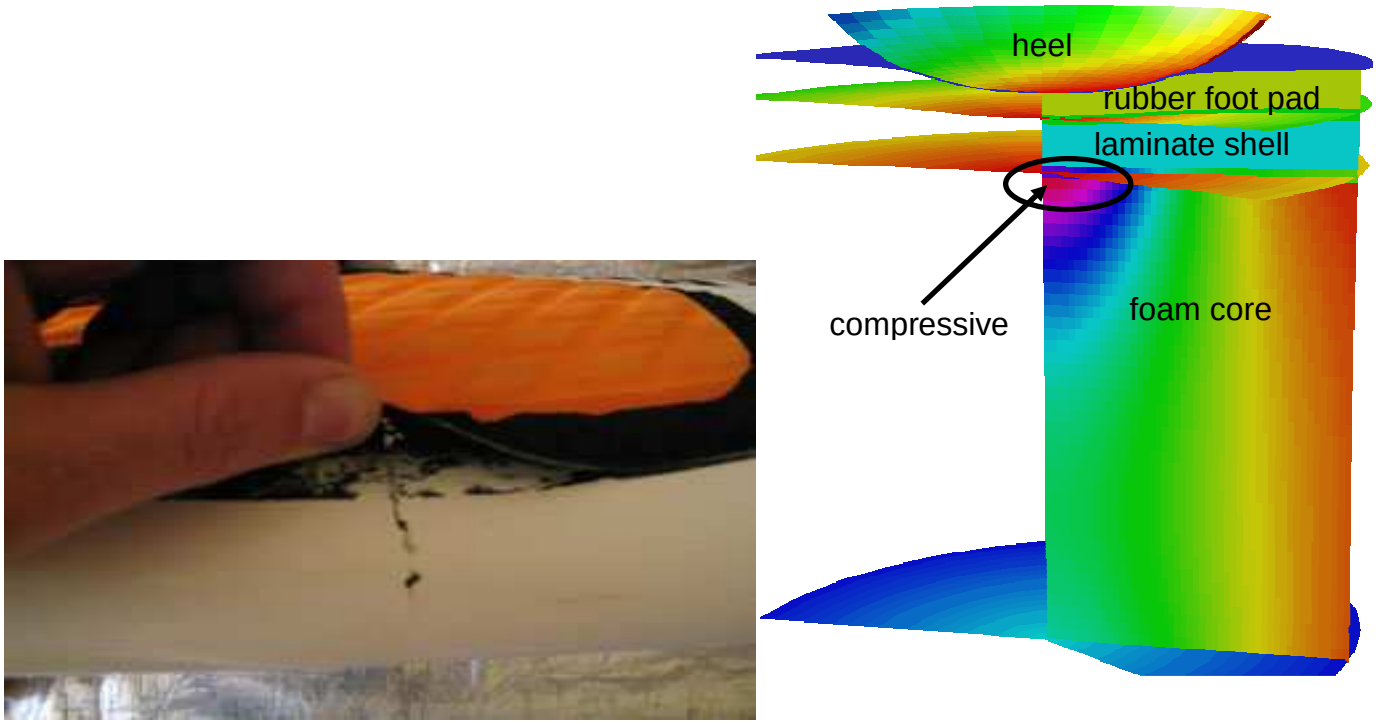

Fig. 7 Impact on the front foot pad (only foam core)

Here elongated or star like cracks coming from the contact centre are observed rather than circular cracks. This becomes clear when we investigate the radial stresses within the laminate under the rider's heel (fig. 7). While, due to the buffer effect of the rubber food pat, there are rather no tensile stresses at the surface of the laminate layer we see, that this time the tensile stress maximum is to be found at the contact centre on the bottom of the laminate shell. But as already seen in problem 1 for the nose part of the board, the foam core is also compressed under the foot pad area due to a maximum of hydrostatic stresses (figure 8):

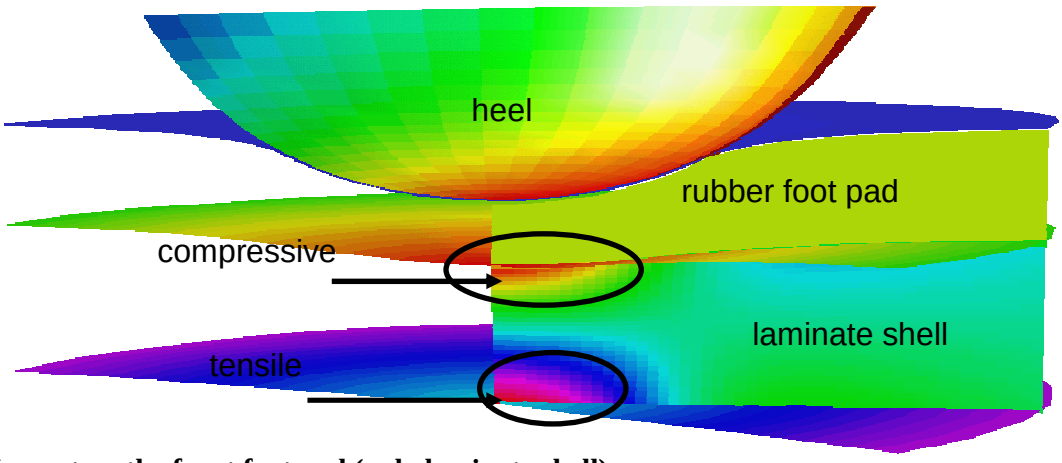

Fig. 8 Impact on the front foot pad (only laminate shell)

This effect is widely known by windsurfers, so that second hand boards are always tested here by simply pressing the thumb hard on the area where usually the heel would be in order to see whether impact damage had already occurred.

In thin film technology a quite similar failure behaviour is known as “star crack formation” (e.g. [20]).

In the case of a “skag hits reef impact” (problem 3, demonstrated in figure 9) the damage (fracture between the front and hind foot straps as shown in figure 9) is caused by high tensile stresses within the board’s surface.

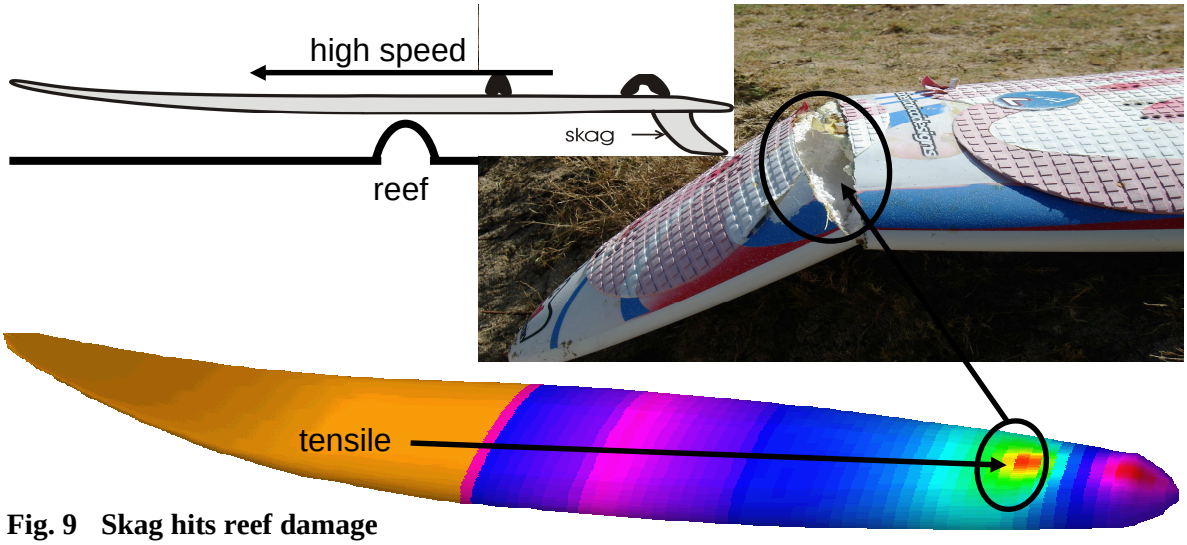

Fig. 9 Skag hits reef damage

To understand why this damage is mainly done on the board surface rather than its bottom one needs to know, that the skag of those thin wave boards considered here is fixed to the

surface. The result can be quite dramatic. In the special case shown in figure 9 the rider has hit an under water obstacle (probably protruding parts of the reef) with the skag of his windsurfing board while fleeing before a huge wave. We see, that depending on the speed of the windsurfer, the impact momentum can be big enough to produce huge tensile stresses in the surface laminate (completely fractured board in figure 9) right in front of the hind foot strap immediately leading to rapture between the two foot pads. This example shows, that our model being originally developed for the investigation of thin film problems in a much smaller scale (microns at the most) still works pretty well even when no obvious thin-film-equivalent can be seen.

The applicability of thin film modelling techniques for even more complex loading conditions including the effects of so called loop jumps, nose dives and hard tail landing has been shown elsewhere [2].

Conclusions

It could be shown on the example of windsurfing boards subjected to a variety of impact loads, that at least a qualitative failure analyses can be performed by using thin film modelling techniques. As these methods are fast and obviously sufficiently accurate in order to predict stress maxima and weak points in the case of typical load distributions of laminate structures, the models might be considered as appropriate tools for the optimisation of these structures. Though, the examples here have been extracted from windsurfing the authors can not see principle obstacles in order to use these techniques in boat hull, automobile body or even fuselage construction, too.

Acknowledgements

The authors are thankful to Rocky Legoy from the RRD-Windsurfing centre on Mauritius, Kevin Berichon from Holly Mackerel Productions, Australia, Stefan Gabler and Holger Schneider, Germany for a variety of helpful discussions and demonstrations. We also want to thank all those riders who damaged their boards, allowed us to interview them in the moment of grieve and even granted us to photograph and thoroughly analyse the board failure.

References

[1] N. Schwarzer: „Modelling of the mechanics of thin films using analytical linear elastic approaches“, habilitation thesis of the TU-Chemnitz 2004, department “Physics of solid bodies”, http://archiv.tu-chemnitz.de/pub/2004/0077

[2] N. Schwarzer, P. Heuer-Schwarzer: „Qualitative failure analysis on laminate structures of windsurfing boards using analytical linear elastic modelling”, Composites Part B: Engineering, submitted December 2004

[3] N. Schwarzer, Arbitrary load distribution on a layered half space, ASME Journal of Tribology, 122 (2000) 672 – 681

[4] H. Gao, C.-H. Chiu, J. Lee, Elastic contact versus indentation modelling of multi-layered materials, Int. J. Solids Structures 29 (1992) 2471-2492

[5] C. Saizonou, R. Kouitat-Njiwa, J. von Stebut, Surface engineering with functionally graded coatings: a numerical study based on the boundary element method, Surf. Coat. Technol. 153 (2002) 290-297

[6] A. E. Giannakopoulos, P. Pallot, J. Mech. Phys. Solids 48 (2000) 1597

[7] A. E. Giannakopoulos, Thin Solid Films 332 (1998) 172

[8] A. E. Giannakopoulos, S. Suresh, Int. J. Solids Structures 34 (1997) 2393

[9] S. M. Aizikovich, V. M. Alexandrov, J .J. Kalker, L. I. Krenev, I. S. Trubchik, Int. J. Solids Structures 39 (2002) 2745

[10] D. S. Stone, J. Mater. Res. 13 (1998) 3207

[11] V. Linss, N. Schwarzer, T. Chudoba, M. Karniychuk, F. Richter: “Mechanical Properties of a Graded BCN Sputtered Coating with VaryingYoung's Modulus: Deposition, Theoretical Modelling and Nanoindentation”, Surf. Coat. Technol., in Press, Corrected Proofs, doi:10.1016/j.surfcoat.2004.06.010

[12] T. Chudoba, N. Schwarzer, V. Linss, F. Richter: „Determination of Mechanical Properties of Graded Coatings using Nanoindentation”, proceedings of the ICMCTF 2004 in San Diego, California, USA, also in Thin Solid Films (2004): 469-470C pp. 239-247

[13] A. I. Lurje: „Three Dimensional Problems of the Theory of Elasticity”, Interscience Publishers, 1964

[14] N. Schwarzer, F. Richter: „On the determination of film stress from substrate bending: STONEY´s formula and its limits“, Microsystem Technologies, submitted November 2004

[15] A. J. Jerri: "Integral and discrete transforms with applications and error analysis", Marcel Dekker, Inc., New York, 1992

[16] V. I. Fabrikant: "Application of potential theory in mechanics: A Selection of New Results", Kluver Academic Publishers, The Netherlands, 1989

[17] ELASTICA, software for the calculation of stresses and deformations in coated systems, ESAE, Germany, free trial version available in the internet at: http://www.esae.de.

[18] FilmDoctor: software for the evaluation of the elastic field of arbitrary combinations of normal and tangential loads of the type “load~ $\sum_{n=1}^{6} c_n * r^n \sqrt{a^2 - r^2}$ ” (with n=0,2,4,6), available at: http://www.siomec.de (contact: contact@siomec.de)

[19] A. Pajares, L. Wei, B. R. Lawn: "Contact damage of plasma sprayed alumina based coatings", Journal of the American Ceramic Society, 79 (1996), 1907 - 1914

[20] A. C. Fischer-Cripps, B. R. Lawn, A. Pajares, L. Wei: Journal of the American Ceramic Society, 79 (1996), 2619 - 2625

Tables

Table 1: Material Parameters for the board's nose part

Layer	A_{11}	A_{12}	A_{13}	A_{33}	A_{44}	Thickness
Transversaly isotropic	$75*E_1$	$15*E_1$	$1.2*E_1$	$1.8*E_1$	$1.6*E_1$	0.5mm
Isotropic	$1.2*E_2$	$0.4*E_2$	$0.4*E_2$	$1.2*E_2$	$0.4*E_2$	2mm
Transversaly isotropic	$75*E_1$	$15*E_1$	$1.2*E_1$	$1.8*E_1$	$1.6*E_1$	0.5mm
Foam core Isotropic	$1.2*E_3$	$0.4*E_3$	$0.4*E_3$	$1.2*E_3$	$0.4*E_3$	82mm
Transversaly isotropic	$75*E_1$	$15*E_1$	$1.2*E_1$	$1.8*E_1$	$1.6*E_1$	0.5mm
Isotropic	$1.2*E_2$	$0.4*E_2$	$0.4*E_2$	$1.2*E_2$	$0.4*E_2$	4mm
Transversaly isotropic	$75*E_1$	$15*E_1$	$1.2*E_1$	$1.8*E_1$	$1.6*E_1$	0.5mm

$E_2=6$ $E_1=100$ $E_3=E$

Table 2: Material Parameters for the board's foot pad area

Layer	A_{11}	A_{12}	A_{13}	A_{33}	A_{44}	Thickness
Rubber pad Isotropic	$1.2*E_0$	$0.4*E_0$	$0.4*E_0$	$1.2*E_0$	$0.4*E_0$	6mm
Transversaly isotropic	$75*E_1$	$15*E_1$	$1.2*E_1$	$1.8*E_1$	$1.6*E_1$	0.5mm
Isotropic	$1.2*E_2$	$0.4*E_2$	$0.4*E_2$	$1.2*E_2$	$0.4*E_2$	3mm
Transversaly isotropic	$75*E_1$	$15*E_1$	$1.2*E_1$	$1.8*E_1$	$1.6*E_1$	0.5mm
Transversaly isotropic	$75*E_1$	$15*E_1$	$1.2*E_1$	$1.8*E_1$	$1.6*E_1$	0.5mm
Isotropic	$1.2*E_2$	$0.4*E_2$	$0.4*E_2$	$1.2*E_2$	$0.4*E_2$	4mm
Transversaly isotropic	$75*E_1$	$15*E_1$	$1.2*E_1$	$1.8*E_1$	$1.6*E_1$	0.5mm
Foam core Isotropic	$1.2*E_3$	$0.4*E_3$	$0.4*E_3$	$1.2*E_3$	$0.4*E_3$	70mm
Transversaly isotropic	$75*E_1$	$15*E_1$	$1.2*E_1$	$1.8*E_1$	$1.6*E_1$	0.5mm
Isotropic	$1.2*E_2$	$0.4*E_2$	$0.4*E_2$	$1.2*E_2$	$0.4*E_2$	4mm
Transversaly isotropic	$75*E_1$	$15*E_1$	$1.2*E_1$	$1.8*E_1$	$1.6*E_1$	0.5mm

$E_2=10$ $E_0=6$ $E_1=100$ $E_3=E$

Table 3: Material Parameters used for the bending load calculation of the skag-hits-reef problem (see text)

Layer	**A_{11}**	**A_{12}**	**A_{13}**	**A_{33}**	**A_{44}**	**Thickness**
Transversaly isotropic	$75*E_1$	$15*E_1$	$1.2*E_1$	$1.8*E_1$	$1.6*E_1$	0.5mm
Isotropic	$1.2*E_2$	$0.4*E_2$	$0.4*E_2$	$1.2*E_2$	$0.4*E_2$	4mm
Transversaly isotropic	$75*E_1$	$15*E_1$	$1.2*E_1$	$1.8*E_1$	$1.6*E_1$	0.5mm
Foam core Isotropic	$1.2*E_3$	$0.4*E_3$	$0.4*E_3$	$1.2*E_3$	$0.4*E_3$	80mm
Transversaly isotropic	$75*E_1$	$15*E_1$	$1.2*E_1$	$1.8*E_1$	$1.6*E_1$	0.5mm
Isotropic	$1.2*E_2$	$0.4*E_2$	$0.4*E_2$	$1.2*E_2$	$0.4*E_2$	4mm
Transversaly isotropic	$75*E_1$	$15*E_1$	$1.2*E_1$	$1.8*E_1$	$1.6*E_1$	0.5mm

$E_2=6$ $E_1=100$ $E_3=E$